

3D-Printed Micro Lens-in-Lens for In Vivo Multimodal Microendoscopy

Jiawen Li,* Simon Thiele, Rodney W. Kirk, Bryden C. Quirk, Ayla Hoogendoorn, Yung Chih Chen, Karlheinz Peter, Stephen J. Nicholls, Johan W. Verjans, Peter J. Psaltis, Christina Bursill, Alois M. Herkommer, Harald Giessen, and Robert A. McLaughlin

Multimodal microendoscopes enable co-located structural and molecular measurements in vivo, thus providing useful insights into the pathological changes associated with disease. However, different optical imaging modalities often have conflicting optical requirements for optimal lens design. For example, a high numerical aperture (NA) lens is needed to realize high-sensitivity fluorescence measurements. In contrast, optical coherence tomography (OCT) demands a low NA to achieve a large depth of focus. These competing requirements present a significant challenge in the design and fabrication of miniaturized imaging probes that are capable of supporting high-quality multiple modalities simultaneously. An optical design is demonstrated which uses two-photon 3D printing to create a miniaturized lens that is simultaneously optimized for these conflicting imaging modalities. The lens-in-lens design contains distinct but connected optical surfaces that separately address the needs of both fluorescence and OCT imaging within a lens of 330 μm diameter. This design shows an improvement in fluorescence sensitivity of $>10\times$ in contrast to more conventional fiber-optic design approaches. This lens-in-lens is then integrated into an intravascular catheter probe with a diameter of 520 μm . The first simultaneous intravascular OCT and fluorescence imaging of a mouse artery in vivo is reported.

usefully characterized at a scale of between tens and hundreds of micrometers. In situ imaging of these changes within the body is the domain of microendoscopy, where a miniaturized imaging device is inserted into the body. To navigate small orifices and lumens of the body, these devices may be required to be sub-millimeter in diameter.

A typical endoscope incorporates a single imaging modality. However, many pathological changes are poorly characterized by a single modality and require additional imaging modalities for accurate diagnosis.^[1–8] Multimodal endoscopes can acquire simultaneous, spatially co-registered measurements of the tissue. For example, high-risk atherosclerotic plaques in cardiovascular disease are often characterized by both a structurally thin fibrous cap and by the presence of autofluorescent intraplaque hemorrhage.^[9] A prototype multimodal endoscopic probe, integrating the structural imaging capabilities of optical coherence tomography (OCT) in

parallel with fluorescence imaging, has demonstrated that there is potential for multimodal endoscopic probes to guide treatments for high-risk plaques,^[6,7,10] which may potentially prevent life-threatening sequelae.^[11,12]


1. Introduction

Diseases are often associated with significant changes in both structure and molecular composition of tissue that can be

J. Li, R. W. Kirk, B. C. Quirk, R. A. McLaughlin
Australian Research Council Centre of Excellence for Nanoscale BioPhotonics
University of Adelaide
Adelaide, SA 5005, Australia
E-mail: jiawen.li01@adelaide.edu.au

J. Li
School of Electrical and Electronic Engineering
University of Adelaide
Adelaide, SA 5005, Australia

J. Li, R. W. Kirk, B. C. Quirk, R. A. McLaughlin
Institute for Photonics and Advanced Sensing
The University of Adelaide
Adelaide, SA 5005, Australia

 The ORCID identification number(s) for the author(s) of this article can be found under <https://doi.org/10.1002/smll.202107032>.

© 2022 The Authors. Small published by Wiley-VCH GmbH. This is an open access article under the terms of the Creative Commons Attribution-NonCommercial License, which permits use, distribution and reproduction in any medium, provided the original work is properly cited and is not used for commercial purposes.

S. Thiele, A. M. Herkommer
Institute of Applied Optics (ITO) and Research Center SCoPE
University of Stuttgart
70569 Stuttgart, Germany

R. W. Kirk, B. C. Quirk, R. A. McLaughlin
School of Biomedicine
University of Adelaide
Adelaide, SA 5005, Australia

A. Hoogendoorn, J. W. Verjans, P. J. Psaltis, C. Bursill
Lifelong Health Theme
South Australian Health and Medical Research Institute (SAHMRI)
Adelaide, SA 5000, Australia

Y. C. Chen, K. Peter
Baker Heart and Diabetes Institute
Melbourne, VIC 3004, Australia

Y. C. Chen, K. Peter
Department of Cardiometabolic Health
Bio21 Institute, Melbourne Medical School
University of Melbourne
Parkville, VIC 3052, Australia

DOI: 10.1002/smll.202107032

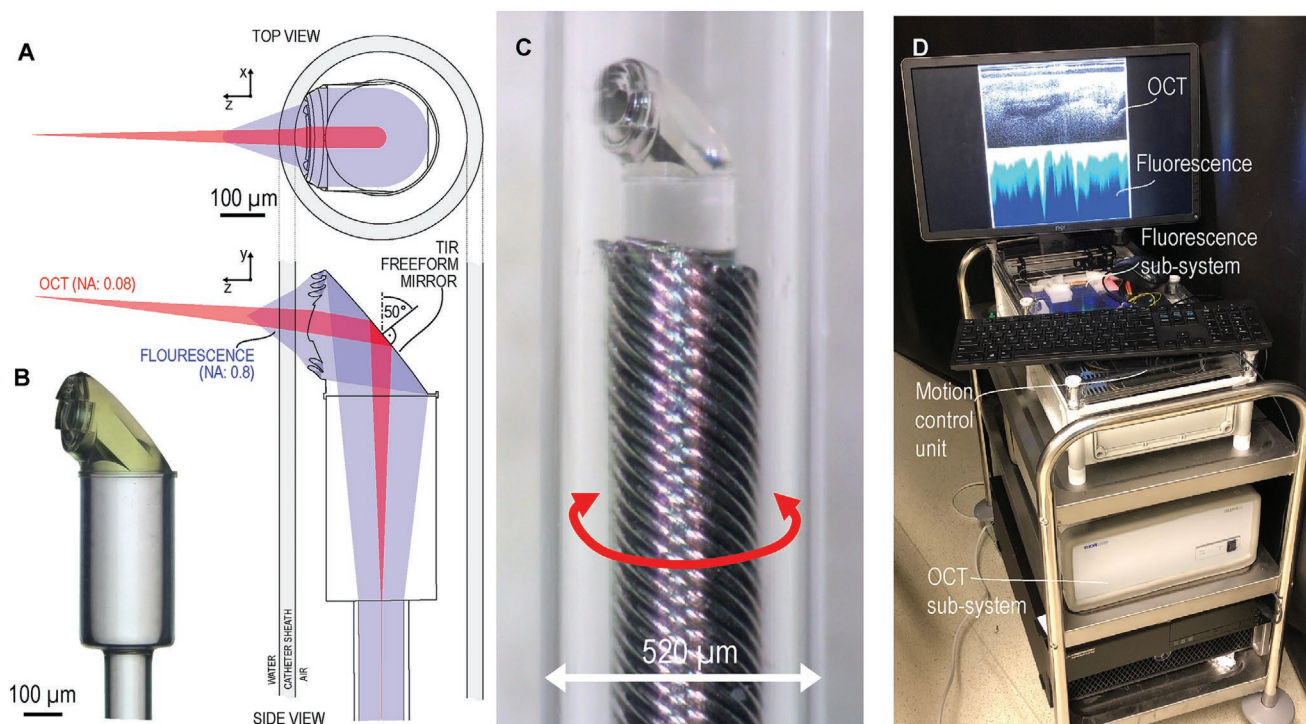


Figure 1. A) Schematic top and side view of the micro lens-in-lens design. B) Digital microscope image of the lens-in-lens directly printed on a no core fiber. C) Microscope image of the 3D printed lens-in-lens endoscopic probe, which includes a metal torque coil and catheter sheath. D) Multimodal OCT+fluorescence system that was integrated with the 3D-printed lens-in-lens endoscopic probe for data acquisition.

Conventionally, these highly miniaturized multimodal endoscopes are often fabricated using a single, monolithic lens that functions poorly for at least one imaging modality. The field of multimodal microendoscopy has been limited because different modalities often have conflicting and incompatible lens-design requirements.^[2,4–6] As a result, performance of at least one imaging modality is compromised. In a multimodal OCT + fluorescence endoscope, a low numerical aperture (NA) lens is typically used to generate a weakly-focused beam to maximize the depth of focus (DOF) of OCT.^[3–5] However, with such a design, the sensitivity of fluorescence detection significantly suffers due to the lens' low acceptance angle. New approaches to design and fabrication are required to integrate a low NA lens that maximizes the OCT imaging range with a

high NA lens that optimizes fluorescence detection sensitivity, whilst still satisfying the sub-millimeter size requirements of in vivo endoscopic imaging. Comparable conflicts exist with other modalities such as video endoscopy or hyperspectral imaging.

3D laser printing has been shown capable of performing precision fabrication of micro-optics.^[13] In particular, two-photon 3D printing allows the creation of sub-millimeter freeform optical designs with sub-micron accuracy, fabricated directly onto the distal tip of an optical fiber.^[14–16] Preliminary work by our team has demonstrated the potential of two-photon 3D printing with single-modality, fiber-optic OCT probes.^[17,18]

In this paper, we describe the use of two-photon 3D printing to address the conflicting optical requirements of multimodal microendoscopic probe design. Exploiting the flexibility of freeform optics, we propose a novel sub-millimeter lens-in-lens design that provides distinct but connected optical surfaces optimized for each modality (**Figure 1A**). Our novel probe comprises an outer lens section to realize a high NA for fluorescence (0.8, to achieve high collection efficiency and sensitivity) and an inner lens section to realize a low NA for OCT (0.08) to achieve a large DOF. Theoretically, the fluorescence sensitivity of our device, which is related to NA, can be up to 100 times higher than that of a device made by a conventional fabrication method.^[3] A sensitivity gain of 13.8 times was measured while a large DOF for OCT was maintained.

To demonstrate the molecular insight that is provided by such a sensitive probe, we have fabricated a miniaturized, multimodal endoscopic probe with a diameter of 0.52 mm including the enclosing catheter (**Figure 1B,C**). We have acquired ex vivo

S. J. Nicholls
Victorian Heart Institute
Monash University
Melbourne, VIC 3168, Australia

J. W. Verjans, P. J. Psaltis
Department of Cardiology
Royal Adelaide Hospital
Adelaide, SA 5000, Australia

J. W. Verjans, P. J. Psaltis
Adelaide Medical School
University of Adelaide
Adelaide, SA 5005, Australia

H. Giessen
4th Physics Institute and Research Center SCoPE
University of Stuttgart
70569 Stuttgart, Germany

multimodal images of a high-risk atherosclerotic plaque in a tandem stenosis (TS) mouse model,^[19,20] using a multimodal OCT+fluorescence system (Figure 1D). This mouse model of cardiovascular disease shows near-infrared autofluorescence (NIRAF), characteristic of intraplaque hemorrhage. To establish the in vivo feasibility of this micro lens-in-lens approach, we subsequently performed in vivo imaging of the diseased aorta of an atherosclerosis-prone apolipoprotein (*Apo*)*E*^{-/-} mouse. This is the first report of intravascular OCT and fluorescence imaging in a mouse artery in vivo.

2. Results and Discussion

2.1. Optical Design of the 3D-Printed Micro Lens-in-Lens

Our OCT+fluorescence probe is based on a double-clad fiber (DCF13, Thorlabs, USA) which consists of a single-mode fiber core; an inner cladding capable of carrying a multimode light signal ($\varnothing = 105 \mu\text{m}$, NA = 0.2), and a second cladding to contain the light within the fiber. Our novel lens-in-lens design optimizes the light from each modality coupled into different parts of the DCF, enabling the use of different NAs for each modality. The OCT light is transmitted to and from the tissue through the fiber core. The fluorescence excitation light is also transmitted to the tissue through the fiber core, but the detected fluorescence emission is coupled into the inner cladding of the fiber. Since the achievable signal-to-noise ratio for fluorescence imaging is directly linked to the NA of the collection cone, a lens with 0.8 NA was designed for coupling light into the inner cladding, which is transferred to the 0.2 NA of the inner cladding through a freeform total internal reflection (TIR) mirror (Figure 1A).

Different types of lenses were investigated for their suitability to be used in a high NA side-viewing configuration for the capture of the fluorescence emission light (Figure 2A). As a promising alternative to more conventional approaches, TIR lenses were identified, which, despite their complex shape, can be easily fabricated by two-photon 3D printing (Figure 2B). In TIR lenses, light is redirected at each of its 'teeth' using TIR and additionally refracted at a second surface (Figure 2C). Using the degrees of freedom of reflection and refraction in a confined space allows highly compact designs with NAs of ≥ 0.8 .^[21] An off-axis lens structure is utilized to make the design compact, reducing the space requirements while maximizing light collection efficiency.

To make off-axis TIR lenses compact and allow the lens-in-lens to fit in a small catheter sheath, a non-rotationally symmetric design can be used. This, however, makes the lens shape and design process complicated.^[22] In order to simplify this, the rotationally symmetric lens (Figure 2D) is separated into three segments with focal lengths $f-s$, f , and $f+s$ that differ by a shift term s . These segments are then combined with a relative displacement s along the optical axis (Figure 2D). For the computation of each segment, a direct surface construction approach was used.^[23] The result is the lens-in-lens shown in Figure 2C in which a central lens (red) is surrounded by a TIR lens (highlighted in pink, yellow, cyan).

An important boundary condition arises from the folding mirror which redirects light from the forward-facing fiber to be

perpendicular to the probe and enables side-viewing (labeled as 'TIR Freeform Mirror' in Figure 1A). The shape of this mirror also collimates light to and from the fiber. Since it is used in TIR (critical angle: 41.5°), sufficient TIR budget must be included to make sure that the whole angular spectrum of the fiber is internally reflected, and surface irregularities do not lead to light leakage. Thus, the TIR mirror is tilted by 50° relatively to the fiber axis resulting in a beam striking the catheter wall at an angle that is 10 degrees from perpendicular.

Altogether, the aperture consists of four different zones as indicated by the colors in Figure 2B: three outer zones (TIR lens) to collect fluorescence emission light, and a central zone (the 'lens in lens') for fluorescence excitation and OCT imaging. This fourth zone (NA: 0.08) compensates the astigmatism introduced by the cylindrical catheter wall for optimal OCT imaging. Note that astigmatism was not corrected in the high NA

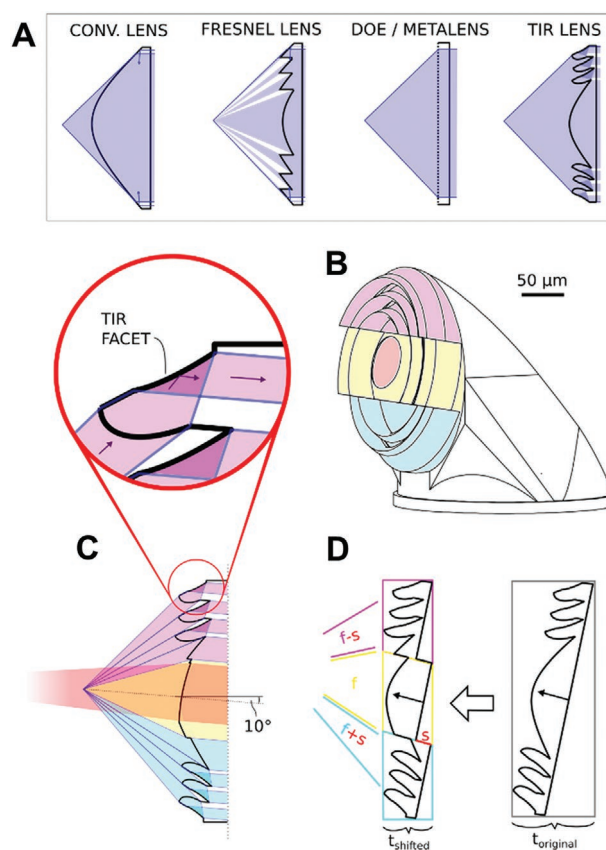


Figure 2. Micro lens-in-lens design. A) Examples of different design forms for the high NA front lens. Conventional lenses exhibit shorter working distances, a limited NA due to TIR, and are less compact. Fresnel lenses enable longer working distances due to their flat form factor but show gaps in the collection cone and have the same NA limitations as conventional lenses. Diffractive optical elements (DOE) and metalenses can have a high NA and be very compact but are currently more inefficient and/or wavelength and/or polarization-sensitive compared to bulk optics,^[24] as well as difficult to fabricate on a side-viewing fiber tip. B) Final design with the different lens regions highlighted. It consists of an inner OCT lens (red) and the TIR lens which is segmented into three parts (pink, yellow, and cyan). C) Sagittal cross-section of the structure which is optimized for an incidence angle of 10° . D) Illustration of TIR lens thickness reduction by segmentation.

outer zones used for fluorescence as diffraction-limited performance is not important for the fluorescence collection path. In pure geometrical terms the faceted nature of the lens does not lead to a loss in collection efficiency as it has a design with no gap in the collection cone. The shifting, however, leads to some small gaps that reduce the overall fluorescence collection efficiency. Although stray light may be generated at the lens surface, the contrast degradation in the OCT path is almost negligible due to the small fiber core diameter and the coherence gating. We anticipate manufacturing inaccuracies (particularly the rounding of sharp edges) and diffraction to have a more significant impact on the collection efficiency compared to the gaps from the lens shifting.

2.2. Fabrication of the Lens-in-Lens Endoscopic Probe

A 450 μm length of no core fiber (NCF) with a glass diameter of $250\pm 10\ \mu\text{m}$ (FG250LA, Thorlabs, USA) was spliced onto the DCF, allowing the light beam from the single-mode core to expand (Figure 1B). The lens-in-lens design was then fabricated directly on the NCF using a two-photon 3D printing system (Photonic Professional GT, Nanoscribe, Germany) and the material Nanoscribe IP-S.^[14,15,25]

A Zeiss Plan-Apochromat 40x/NA1.4 objective lens was used for the 3D printing. Printing was performed using the following parameters: laser power setting of 42.5%; scan speed of $25,000\ \mu\text{m}\ \text{s}^{-1}$; slicing distance of $0.1\ \mu\text{m}$; hatching distance of $0.15\ \mu\text{m}$. After printing, the part was developed in mr-Dev 600 solution (micro resist technology GmbH, Germany) for 20 min followed by rinsing in isopropyl alcohol for 2 min. No further post-processing was necessary. Analysis of surface quality in our previous studies have shown that these parameters typically result in shape accuracies of $<1\ \mu\text{m}$ and a surface roughness of $\approx 10\ \text{nm}\ \text{RMS}$.^[1]

After 3D printing of the lens-in-lens, this fiber-lens assembly was housed within a metal coil (ACTONE, ASAHI Intecc Co., Ltd., Japan) to enable reliable probe rotation, and enclosed within a transparent catheter sheath (material: fluorinated ethylene propylene; inner diameter: $0.41\ \text{mm}$; outer diameter: $0.52\ \text{mm}$; Zeus Inc., USA) for protection during rotation within a blood vessel (Figure 1C).^[17,27] Note that OCT imaging using DCF is prone to artifacts due to cross-coupling of light between the fiber core and inner cladding which can create a ghost image when short lengths of DCF fiber are used.^[28] Accordingly, the length of DCF fiber used in the probe was kept at over 2 m in length to minimize these effects.^[29] Sterilization of the device was not required in this application. However, our internal studies have shown the photoresist IP-S to be stable up to over $150\ ^\circ\text{C}$, making it suitable for sterilization using an approach such as vaporized hydrogen peroxide gas plasma sterilization (STERRAD, Advanced Sterilization Products, USA), as used in other human in vivo fiber-optic probe studies by our group,^[30] or autoclaving in hot pressurized water vapor at $134\ ^\circ\text{C}$.

2.3. Characterization

The endoscopic probe was first characterized by profiling the emitted OCT light beam in water,^[17] which mimics the

biological aqueous environment. The setup for beam profiling this probe in water is shown in Figure S1, Supporting Information. The beam at the focal point of the OCT path is shown in the inset of Figure 3C, the FWHM diameter of which is $9.8\ \mu\text{m}$. The effective depths of focus (the depth range in which $\text{FWHM} < 2\text{FWHM}_{\text{min}}$)^[31] of $570\ \mu\text{m}$ (x axis) and $680\ \mu\text{m}$ (y axis). We attribute slight astigmatism due to imperfections in the 3D printing process for a lens that is oriented at approximately 90° to the writing axis, possibly because the writing voxels are not spherical but elliptical. The beam diameter and effective depths of focus are of comparable values to previously published DCF probes.^[3,32]

The sensitivity of the probe in detecting fluorescence signal was quantified in comparison to a more conventional fiber-probe whose fabrication involved spliced lengths of graded-index (GRIN) and NCF fiber, with a published design.^[3] The comparison used the setup detailed in Figure S2, Supporting Information. As illustrated in Figure 3D, the 3D printed lens-in-lens design achieved a 13.8-fold sensitivity gain in fluorescence detection when compared to the conventional probe design.

2.4. 3D Ex Vivo Imaging of a High-Risk Plaque in a Mouse Model

Mouse models offer the ability to study complicated diseases systematically as they are affordable with low genetic variation, and molecular mechanisms can be definitively tested using genetic modifications such as gene knock-out or transgenic overexpression. The *ApoE*^{-/-} TS murine model uniquely reflects histological atherosclerotic plaque instability that is comparable to humans (including plaque rupture, thin fibrous cap, localized inflammation, and intraplaque hemorrhage).^[33] Figure 4 depicts OCT+fluorescence images of a TS murine carotid artery acquired using the lens-in-lens probe ex vivo. The OCT+fluorescence images were obtained by the set up illustrated in Figure S3, Supporting Information. The detection of NIRAF with miniaturized imaging probes has previously been challenging as the autofluorescence signal is weak, requiring high laser power or long image acquisition times for appropriate detection.^[19] Here, the improved sensitivity provided by the high NA of the TIR lens incorporated into the lens-in-lens design has enabled the mapping of autofluorescence signals of the artery with a tissue-safe laser power. In particular, our results show a high NIRAF signal at the proximal end of the TS region (yellow arrow), which colocalized with the high-risk plaque and perivascular scar tissue. This result matches what has previously only been visible using a large, bench-top fluorescence microscope,^[19] but has not previously been visible using a miniaturized endoscopic probe.

2.5. 3D Intravascular Imaging of a Diseased Mouse Artery In Vivo

In vivo intravascular structural and fluorescence imaging of plaque development in mouse arteries have previously not been feasible due to the extremely small diameter of mouse arteries and the challenges in fabricating high sensitivity, miniaturized endoscopic probes.

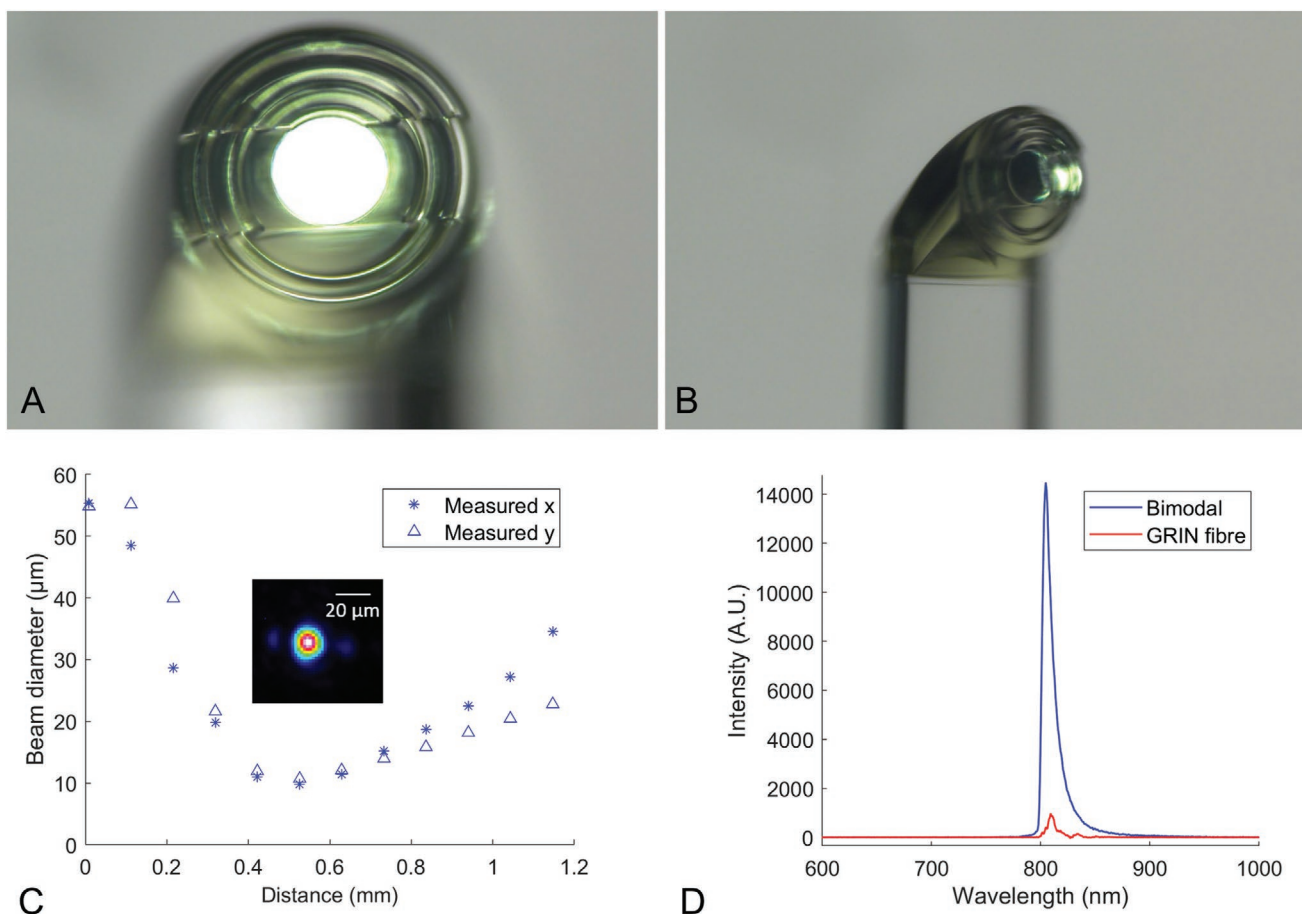


Figure 3. Characterization of both OCT and fluorescence channels. Microscopic images of the 3D printed lens, show both A) on-axis view and B) off-axis view. C) Beam profiles (FWHM) obtained from the 3D printed micro lens-in-lens with the catheter, indicating negligible astigmatism (coordinates shown in Figure 1), Inset focal spot profile; D) Comparison of collected ICG fluorescence signals by a 3D printed lens-in-lens endoscope and GRIN-fiber-based endoscope. Note that backgrounds have been subtracted. The diluted Indocyanine green (ICG) solution has a concentration of 0.25 mg L^{-1} .

By utilizing the lens-in-lens design, we have demonstrated *in vivo* imaging of a mouse artery (**Figure 5**). To the best of our knowledge, this is the first time that multimodal structural (i.e., OCT) and high-sensitivity fluorescence images have been acquired from inside an artery of a living mouse.

Unlike our earlier *ex vivo* sample (Figure 4), this living mouse did not manifest a plaque that is high-risk and prone to cause life-threatening sequelae. As a result, there is no significant NIRAF signal. In this animal, we utilized indocyanine

green (ICG) as a fluorescence contrast agent to highlight the atherosclerotic pathology present in the vessel.^[34] ICG was injected 1 h prior to the *in vivo* imaging procedure, allowing uptake by the vessel walls. OCT+fluorescence results acquired with the lens-in-lens design were compared against those acquired using a more conventionally fabricated probe using a GRIN fiber lens.^[3] After *in vivo* imaging, the vessel was excised for histological analysis.

A 3D volume-rendered image of the blood vessel is shown in Figure 5A, reconstructed from the OCT data acquired using the

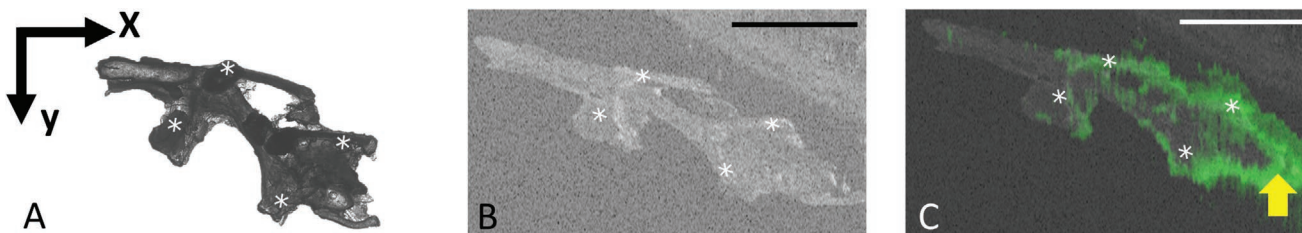


Figure 4. *Ex vivo* imaging of mouse high-risk plaque. A) photo of the TS murine carotid artery B) en face OCT image of the TS artery (* indicate suture material); C) Co-localized OCT (grey) and fluorescence (green) image of a TS artery acquired by the 3D printed lens-in-lens endoscope *ex vivo*. Yellow arrow points to the high autofluorescence signal likely to be generated by a high-risk plaque and perivascular scar tissue. Scale bar: $100 \mu\text{m}$.

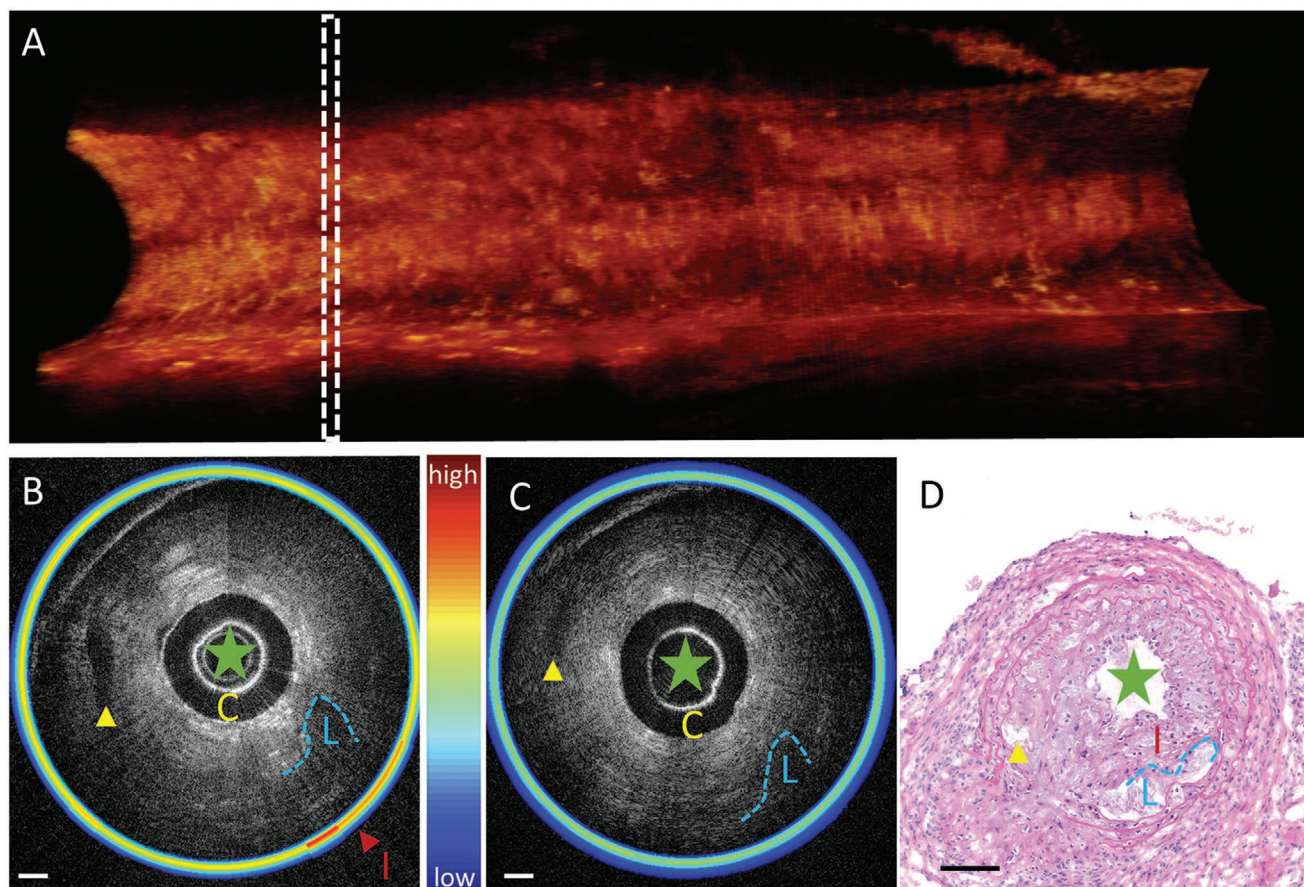


Figure 5. In vivo imaging of diseased mouse artery. A) 3D volume rendering of the OCT data set of the diseased artery obtained with the lens-in-lens endoscopic probe. This volume-rendered image is constructed from 195 OCT B-scans with the data cropped through the center of the vessel to show the vessel lumen, visualized using a lookup table (LUT) colormap. B) OCT (grey) and fluorescence (color) cross-sections of the mouse artery from the white dashed region in (A), imaged with the lens-in-lens probe. The greyscale OCT image shows a radial B-scan, whilst the fluorescence signal shows the accumulated fluorescence signal at each radial position, visualized using the color scale shown. The red triangle marks a localized high fluorescence signal (red), indicating inflammation in those regions of the plaque. The boundary between the lipid-rich necrotic core and the fibrous region is highlighted by the blue dashed line. The lumen of the artery and a void are denoted by a green star and yellow arrow, respectively. C) Cross-sectional OCT and fluorescence images acquired using a conventional GRIN fiber lens probe from the same location as (B), showing less fluorescence sensitivity. D) Corresponding H&E histology image. C: catheter sheath; L: lipid-rich necrotic core; I: Inflammation. Scale bar: 100 μm .

lens-in-lens probe. The dashed white box in Figure 5A indicates a location within the plaque, and the OCT+fluorescence cross-sectional images from that location are shown below. Figure 5B was acquired using the lens-in-lens probe, and Figure 5C using the conventional GRIN fiber lens probe.^[3] The OCT data are shown in greyscale, bounded by the color-coded fluorescence intensity signal. Note that the OCT data are depth-resolved, providing an entire structural image. The fluorescence signal is a projection image, with an accumulated measurement at each radial position. This is graphically represented by the colored circle, with variations in color indicating changes in fluorescence. A hematoxylin and eosin (H&E)-stained histology section from the same location is shown in Figure 5D.

In the OCT images, comparable features are visible in both the image acquired using the lens-in-lens design (Figure 5B) and a conventional GRIN fiber lens design (Figure 5C), validating that the scans are examining the same location in the blood vessel. These features include a diffuse area of reduced optical scattering corresponding to the lipid pool of the plaque,

delineated with a dashed blue line and marked L for lipid. A small and distinctive area of reduced backscatter is also visible in both scans and marked with a yellow triangle. The cross-section of the imaging catheter is labeled C and the lumen center is marked with a green star. Corresponding features are labeled in the matching histology in Figure 5D.

The histological section also shows an area of inflammation, labeled with a red I. Because of the high sensitivity of the lens-in-lens probe, this is detected as an area of increased fluorescence in Figure 5B and marked with a red arrow at the 5 o'clock location. The less sensitive, conventional GRIN fiber lens is unable to detect the variation in fluorescence, and the feature is not visible in Figure 5C. This is because the conventional lens is optimized for OCT scanning using a low NA, to the detriment of fluorescence sensitivity which would require a high NA lens. The improved ability to detect variations in the fluorescence, whilst maintaining comparable OCT image quality, highlights the value of adopting an approach such as the lens-in-lens design, where the probe can be simultaneously

optimized for the conflicting optical requirements of multiple modalities.

3. Conclusion

In this study, we demonstrated a freeform lens-in-lens design fabricated using two-photon 3D printing. This design allows independent optimization of the imaging optics for multiple imaging modalities with conflicting requirements. The approach enables the fabrication of highly miniaturized imaging probes that deliver high performance across multiple modalities. By incorporating this lens-in-lens design, a large DOF in the OCT channel (>500 μm by a low NA of 0.08) is achieved in parallel with a high NA ($= 0.8$) for fluorescence detection. The >10x sensitivity gain realized by this micro lens-in-lens enables in vivo OCT+fluorescence to be achieved with a lower laser power and a lower concentration of fluorescent dye, reducing dye toxicity. These technical innovations have been incorporated into a novel multimodal endoscopic imaging probe, with an outer diameter of 0.52 mm (including the enclosing transparent catheter). The sensitivity of this probe was sufficient to image the NIRAF indicative of high-risk atherosclerotic plaques in a mouse model, previously only visualized using substantially larger microscope optics. Development of such a small imaging probe has also enabled the first in vivo OCT+fluorescence images acquired inside a mouse vessel detecting fluorescent markers of disease with high sensitivity.

4. Experimental Section

OCT+Fluorescence Imaging System: The multimodal system (Figure 1D and Figure S4, Supporting Information) consisted of fluorescence and OCT sub-systems, and a custom motion control unit. The fluorescence and OCT sub-systems were integrated through a customized coupler module, including a wavelength division multiplexer and DCF coupler (Castor Optics Inc., Canada), and synchronized by the trigger signal from the motion control unit.

For the fluorescence sub-system, excitation light from a 783 nm laser (MatchBox, Integrated Optics, Lithuania) was delivered into the DCF coupler unit and then into the DCF fiber-optic imaging probe. The detected fluorescence signal was extracted from the inner cladding of the DCF and coupled into a multimode output fiber by the DCF coupler. This was then filtered with a long pass filter (FELH0800, Thorlabs, USA) and detected using a portable spectrometer (QE Pro, Ocean Optics, USA).

For the OCT sub-system, a commercially-available spectral-domain OCT system (Teleso II, Thorlabs GmbH, Germany) with a central wavelength of 1300 nm and an axial resolution of 5.5 μm (in air) was used.

The main components of the motion control unit were a counter-rotation motor to rotate the imaging probe through 360 degrees during image acquisition,^[35] and a motorized linear stage to pull-back the fiber probe, enabling acquisition of a 3D data volume along a section of a blood vessel in vivo.

Ex vivo high-risk plaque x-y raster-scanned image (Figure 4) was obtained by using two motorized linear translation stages, as shown in Figure S3, Supporting Information. The distance between steps in the x axis was 0.02 mm.

In Vivo Mouse Experiment: Animal studies were approved by South Australia Health Medical Research Institute Animal Ethics Committee (SAM425.19).

To enable in vivo intravascular imaging in a mouse, the carotid interposition grafting mouse model was performed.^[36] In this model, the thoracic aorta (approximately 10-mm in length) from a donor mouse was interposition-grafted into the right common carotid artery of a recipient mouse. This model allows to image the largest artery (thoracic aorta) in a mouse with an inner diameter of 1.2–1.3 mm, similar to that of a mid-distal end of human coronary artery. Furthermore, placing the thoracic aorta in the carotid region enables survival studies, as clamping of the right carotid artery can be performed whilst imaging without causing death as blood supply was maintained to the brain via the neighboring left carotid artery. An eight-week-old *ApoE*^{-/-} mouse was put on a high-fat diet for 43 weeks to develop advanced atherosclerotic plaques in the thoracic aorta. After this period, this donor mouse was euthanized, and its thoracic aorta (with plaques) was excised and grafted into the carotid-region of a recipient mouse. Note that the *ApoE*^{-/-} recipient mouse had also been fed a high-fat diet 6 weeks prior to surgery. Following the carotid interposition grafting surgery, the high-fat diet was continued for a further 6 weeks to allow full recovery of the grafted region. Following this, in vivo intravascular imaging was performed. One hour prior to the imaging experiment, ICG (with a concentration of 500 $\mu\text{g kg}^{-1}$) was injected via the tail vein. For the imaging procedure, the mouse was anesthetized with isoflurane. The grafted aorta was once again isolated and clamped at the proximal and distal ends. A small transverse arteriotomy was made in the graft through which the 3D-printed lens-in-lens endoscopic probe was inserted. Subsequently, OCT+fluorescence imaging using the probe was performed.

Supporting Information

Supporting Information is available from the Wiley Online Library or from the author.

Acknowledgements

The authors acknowledge National Health and Medical Research Council (NHMRC) Ideas Grant (APP2001646 and APP2002254), the Australian Research Council (CE140100003), BMBF PRINTOPTICS (13N14096, 13N14097) and QR.X, Baden-Württemberg (BW) Stiftung OPTERIAL, European Research Council Advanced Grant COMPLEXPLAS, European Research Council Proof of Concept 3D Printed Optics, German Research Foundation (DFG), Integrated quantum science and technology (IQST), and Australia-Germany Joint Research Co-operation Scheme (UA-DAAD). University of Stuttgart Terra Incognita Fund. J.L. was the recipient of Fellowships from National Heart Foundation of Australia (102093 and 105608) and NHMRC Investigator EL1 Fellowship (GNT2008462). A.H. was the recipient of a Netherlands Heart Institute Fellowship (2018). Y.C.C. was the recipient of a Future Leader Fellowship from the National Heart Foundation of Australia (102068). K.P. was the recipient of a NHMRC Investigator L3 Fellowship (GNT1174098). S.J.N. was the recipient of a NHMRC Principal Research Fellowship (1111630). C.A.B. was the recipient of Lin Huddleston Senior Fellowship from the National Heart Foundation of Australia. C.A.B. and R.A.M. acknowledge NHMRC Development Grant (APP1178912). P.J.P. was the recipient of a Future Leader Fellowship from the National Heart Foundation of Australia (FLF102056) and a Career Development Fellowship from the NHMRC (CDF1161506).

Conflict of Interest

Y.C.C. and K.P. are inventors on a patent describing NIRAF for the detection of high-risk, rupture-prone atherosclerotic plaques. K.P. is the chief medical officer of NIRTEK. R.W.K., B.C.Q., and R.A.M. are co-founders and directors of Miniprobe Pty Ltd., a company that

develops novel optical imaging systems. Miniprobes Pty Ltd. did not contribute to this study. S.J.N. has received research support from AstraZeneca, Amgen, Anthera, CSL Behring, Cerenis, Eli Lilly, Esperion, Resverlogix, Novartis, InfraRedx, and Sanofi-Regeneron and is a consultant for Amgen, Akcea, AstraZeneca, Boehringer Ingelheim, CSL Behring, Eli Lilly, Esperion, Kowa, Merck, Takeda, Pfizer, Sanofi-Regeneron, and Novo Nordisk. P.J.P. has received research support from Abbott Vascular, consulting fees from Amgen and Esperion and speaker honoraria from AstraZeneca, Bayer, Boehringer Ingelheim, Merck Schering-Plough, and Pfizer.

Data Availability Statement

The data that support the findings of this study are available from the corresponding author upon reasonable request.

Keywords

3D printing, multimodal imaging, near infrared fluorescence, optical coherence tomography, two-photon laser lithography

Received: November 14, 2021

Revised: January 19, 2022

Published online: March 1, 2022

- [1] S. Liang, A. Saidi, J. Jing, G. Liu, J. Li, J. Zhang, C. Sun, J. Narula, Z. Chen, *J. Biomed. Opt.* **2012**, *17*, 0705011.
- [2] H. Pahlevaninezhad, A. M. D. Lee, G. Hohert, S. Lam, T. Shaipanich, E.-L. Beaudoin, C. MacAulay, C. Boudoux, P. Lane, *Opt. Lett.* **2016**, *41*, 3209.
- [3] L. Scolaro, D. Lorenser, W.-J. Madore, R. W. Kirk, A. S. Kramer, G. C. Yeoh, N. Godbout, D. D. Sampson, C. Boudoux, R. A. McLaughlin, *Biomed. Opt. Express* **2015**, *6*, 1767.
- [4] H. Yoo, J. W. Kim, M. Shishkov, E. Namati, T. Morse, R. Shubochkin, J. R. McCarthy, V. Ntziachristos, B. E. Bouma, F. A. Jaffer, G. J. Tearney, *Nat. Med.* **2011**, *17*, 1680.
- [5] H. Wang, J. A. Gardecki, G. J. Ughi, P. V. Jacques, E. Hamidi, G. J. Tearney, *Biomed. Opt. Express* **2015**, *6*, 1363.
- [6] G. J. Ughi, H. Wang, E. Gerbaud, J. A. Gardecki, A. M. Fard, E. Hamidi, P. Vacas-Jacques, M. Rosenberg, F. A. Jaffer, G. J. Tearney, *JACC: Cardiovasc. Imaging* **2016**, *9*, 1304.
- [7] J. W. Verjans, E. A. Osborn, G. J. Ughi, M. A. C. Press, E. Hamidi, A. P. Antoniadis, M. I. Papafaklis, M. F. Conrad, P. Libby, P. H. Stone, *JACC: Cardiovasc. Imaging* **2016**, *9*, 1087.
- [8] J. Li, N. J. Montarello, A. Hoogendoorn, J. W. Verjans, C. A. Bursill, K. Peter, S. J. Nicholls, R. A. McLaughlin, P. J. Psaltis, *JACC: Cardiovasc. Imaging* **2022**, *15*, 145.
- [9] M. Naghavi, P. Libby, E. Falk, S. W. Casscells, S. Litovsky, J. Rumberger, J. J. Badimon, C. Stefanadis, P. Moreno, G. Pasterkamp, *Circulation* **2003**, *108*, 1772.
- [10] S. Kim, M. W. Lee, T. S. Kim, J. W. Song, H. S. Nam, H. S. Cho, S.-J. Jang, J. Ryu, D. J. Oh, D.-G. Gweon, S. H. Park, K. Park, W.-Y. Oh, H. Yoo, J. W. Kim, *Eur. Heart J.* **2016**, *37*, 2833.
- [11] S. Waxman, F. Ishibashi, J. E. Muller, *Circulation* **2006**, *114*, 2390.
- [12] J. L. Fleg, G. W. Stone, Z. A. Fayad, J. F. Granada, T. S. Hatsukami, F. D. Kolodgie, J. Ohayon, R. Pettigrew, M. S. Sabatine, G. J. Tearney, S. Waxman, M. J. Domanski, P. R. Srinivas, J. Narula, *JACC: Cardiovasc. Imaging* **2012**, *5*, 941.
- [13] S. Lightman, G. Hurvitz, R. Gvishi, A. Arie, *Appl. Opt.* **2017**, *56*, 9038.
- [14] T. Gissibl, S. Thiele, A. Herkommer, H. Giessen, *Nat. Commun.* **2016**, *7*, 11763.
- [15] T. Gissibl, S. Thiele, A. Herkommer, H. Giessen, *Nat. Photonics* **2016**.
- [16] M. Plidschun, H. Ren, J. Kim, R. Förster, S. A. Maier, M. A. Schmidt, *Light: Sci. Appl.* **2021**, *10*, 57.
- [17] J. Li, S. Thiele, B. C. Quirk, R. W. Kirk, J. W. Verjans, E. Akers, C. A. Bursill, S. J. Nicholls, A. M. Herkommer, H. Giessen, R. A. McLaughlin, *Light: Sci. Appl.* **2020**, *9*, 124.
- [18] J. Li, P. Fejes, D. Lorenser, B. C. Quirk, P. B. Noble, R. W. Kirk, A. Orth, F. M. Wood, B. C. Gibson, D. D. Sampson, R. A. McLaughlin, *Sci. Rep.* **2018**, *8*, 14789.
- [19] N. M. Htun, Y. C. Chen, B. Lim, T. Schiller, G. J. Maghzal, A. L. Huang, K. D. Elgass, J. Rivera, H. G. Schneider, B. R. Wood, R. Stocker, K. Peter, *Nat. Commun.* **2017**, *8*, 75.
- [20] J. Noonan, A. Bobik, K. Peter, *Br. J. Pharmacol.* **2020**, *179*, 979.
- [21] A. Siniscalco, in *New Frontiers for Design of Interior Lighting Products* (Ed: A. Siniscalco), Springer International Publishing, Cham, **2021**, pp 103–128.
- [22] W. Parkyn, W. Falicoff, J. Minano, P. Benitez, J. Chavez, Y. Sun, Proc. SPIE 5186, Design of Efficient Illumination Systems, **2003**.
- [23] S. Thiele, *Ph.D. thesis*, University of Stuttgart, **2019**.
- [24] P. Lalanne, P. Chavel, *Laser Photonics Rev.* **2017**, *11*, 1600295.
- [25] H. Giessen, M. Thiel, T. Gissibl, *WO2017059960A1*, **2015**.
- [26] T. Gissibl, *Ph.D. thesis*, University of Stuttgart, **2016**.
- [27] M. J. Gora, M. J. Suter, G. J. Tearney, X. Li, *Biomed. Opt. Express* **2017**, *8*, 2405.
- [28] A. Tanskanen, G. Hohert, A. Lee, P. M. Lane, *J. Lightwave Technol.* **2021**, *39*, 5573.
- [29] K. Beaudette, H. W. Baac, W.-J. Madore, M. Villiger, N. Godbout, B. E. Bouma, C. Boudoux, *Biomed. Opt. Express* **2015**, *6*, 1293.
- [30] H. Ramakonar, B. C. Quirk, R. W. Kirk, J. Li, A. Jacques, C. R. P. Lind, R. A. McLaughlin, *Sci. Adv.* **2018**, *4*, eaav4992.
- [31] D. Lorenser, X. Yang, D. D. Sampson, *Opt. Lett.* **2012**, *37*, 1616.
- [32] K. Beaudette, M. Strupler, J. Ren, B. E. Bouma, C. Boudoux, *Appl. Opt.* **2018**, *57*, 1110.
- [33] Y.-C. Chen, A. V. Bui, J. Diesch, R. Manasseh, C. Hausding, J. Rivera, I. Haviv, A. Agrotis, N. M. Htun, J. Jowett, C. E. Hagemeyer, R. D. Hannan, A. Bobik, K. Peter, *Circ. Res.* **2013**, *113*, 252.
- [34] J. W. Verjans, E. A. Osborn, G. J. Ughi, M. A. C. Press, E. Hamidi, A. P. Antoniadis, M. I. Papafaklis, M. F. Conrad, P. Libby, P. H. Stone, *JACC: Cardiovasc. Imaging* **2016**, *9*, 1087.
- [35] B. C. Quirk, R. A. McLaughlin, A. Curatolo, R. W. Kirk, P. B. Noble, D. D. Sampson, *J. Biomed. Opt.* **2011**, *16*, 036009.
- [36] L. Z. Vanags, J. T. M. Tan, K. K. Galougahi, A. Schaefer, S. G. Wise, A. Murphy, Z. A. Ali, C. A. Bursill, *JACC: Basic Trans. Sci.* **2018**, *3*, 200.